analytical chemistry

pubs.acs.org/ac Article

Molecular Examination of Ion-Pair Competition in Alkaline Aluminate Solutions Using In Situ Liquid SIMS

Yining Wang, Duo Song, Yadong Zhou, Cuixia Cheng, Yanyan Zhang, Carolyn I. Pearce, Zheming Wang, Sue B. Clark, Junwu Zhu,* Kevin M. Rosso,* Zihua Zhu,* and Xin Zhang*

Cite This: *Anal. Chem.* 2021, 93, 1068−1075 Read Online

ACCESS | Metrics & More | Article Recommendations | Supporting Information

ABSTRACT: Understanding the structure and composition of aluminate complexes in extremely alkaline systems such as Bayer liquors has received enormous attention due to their fundamental and industrial importance. However, obtaining direct molecular information of the underlying ion−ion interactions using traditional approaches such as NMR spectroscopy or Raman spectroscopy is challenging due to the weakness of these interactions and/or their complex overlapping spectral signatures. Here, we exploit in situ liquid secondary-ion mass spectrometry (SIMS) as a new approach and show how it enables new insights. In contrast with traditional techniques, using SIMS we succeeded in acquiring information on dominant ion clusters in these alkaline systems. In Na^+/K^+ mixed alkaline aluminate solutions, we clearly observe preferential formation of Na^+-anion clusters over K^+-anion clusters. Evaluation of these clusters by density functional theory (DFT) calculations shows that these structures are stable and that their relative bond energies are consistent with their observed SIMS signal intensity differences. This demonstrates a key advantage of in situ liquid SIMS for overcoming ambiguities obscuring important information in these systems on constituent molecular clusters defined by relatively weak ion-pair competition and ion−solvent interactions.

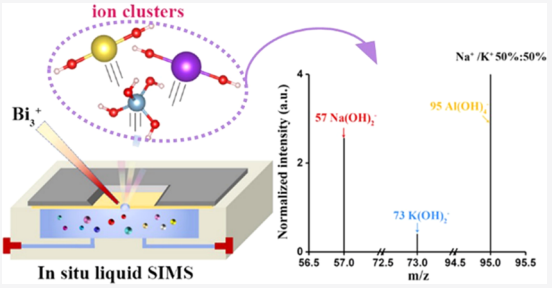

INTRODUCTION

Understanding ion pairing of simple oppositely charged ions in electrolyte solutions and the effect of counterions on ion-pair formation is critical for material synthesis, catalysis, energy storage, environmental conservation, biological medicine, and so on.[1−7] For example, formation of ion pairs can enhance the separation of organic molecules such as peptides and proteins from natural products and thus is a widely employed strategy in the preparation and analysis of pharmaceuticals.[2,8−11] Likewise, the desirable properties of phosphors can be promoted by optimizing the concentration of ion pairs between rare earth element dopants and counterions to improve the energy transfer.[5] Moreover, crystal phases and their relative growth rates can be controlled by introducing different counterions to adjust the ion-pair formation behavior.[3,6,12,13]

To date, extensive experimental techniques have been employed to explore ion-pairing phenomena. The most popular method is characterization of changes in local chemical bonding environments using various spectroscopy-based measurements, such as NMR spectroscopy,[7,14,15] electron paramagnetic/spin resonance (EPR),[16−18] infrared spectroscopy (IR),[19] Raman spectroscopy,[19−21] sum frequency spectroscopy (SFG),[22−24] UV−vis,[17,25] fluorescence,[26] nonlinear optics,[27] and dielectric spectroscopy.[28] Generally, the determination of ion pairing using these spectroscopic techniques depends on the observation of a new peak or the shift of an original peak as a result of the formation of a new species in the system.[1] Another popular method is based on examining the variation of structural parameters such as the $M^{\delta+}-N^{\delta-}$, $M^{\delta+}-H_2O$, $M^{\delta+}-O$, $N^{\delta}-H_2O$, OH−OH, and H_2O-H_2O distances using X-ray absorption spectroscopy (XAS),[14,29−31] X-ray wide/small angle scattering (WAXS/SAXS),[32] X-ray diffraction (XRD),[33] neutron scattering,[3] and so on. In addition, less common methods such as electrical conductivity, potentiometric, thermodynamic, relaxation, and viscosity measurements have also been used to investigate ion pairs.[34−36] Although useful, in complex multicomponent solutions, especially highly concentrated ones, most of these techniques suffer from ambiguities arising from multiple overlapping signals, particularly the difficulty of isolating weakly bound species with clear molecular recognition.

Given these limitations, much of our current knowledge on possible molecular structures of ion pairs is based upon molecular computational efforts.[37−44] However, these ap-

Received: September 27, 2020
Accepted: November 24, 2020
Published: December 7, 2020

https://dx.doi.org/10.1021/acs.analchem.0c04070
Anal. Chem. 2021, 93, 1068−1075

proaches also suffer from necessary approximations to either reduce system complexity or embrace less accurate methods to manage computational expense. For instance, the simulations may have to be performed in a vacuum in the absence of the surrounding medium or with a reduced simulation cell or overall physio-chemical scope of the problem. Classical molecular dynamics (MD) simulations have been a versatile approach but often cannot completely encompass all possible bond breaking and making events that impact cluster formation pathways.[45] Although modeling remains very useful, reliance on this approach reinforces the importance of obtaining straightforward experimental evidence to verify model correctness.

For this purpose, we recently developed an innovative in situ liquid secondary-ion mass spectrometry (SIMS) approach (Figure 1) that allows us to directly analyze the surface of

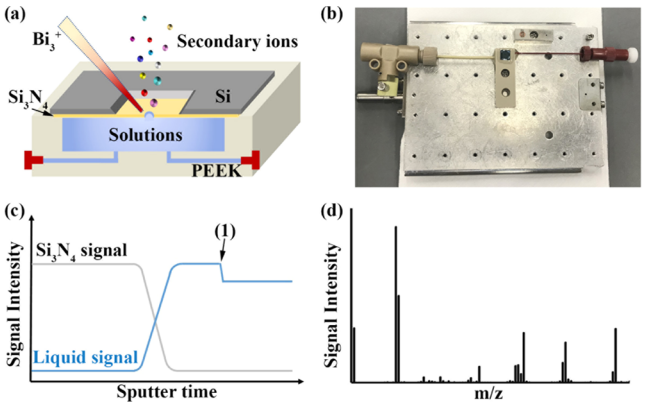

Figure 1. (a) Schematic illustration of the in situ liquid SIMS measurement of liquid samples. (b) Photograph of a real assembled liquid cell device on the sample holder for further SIMS analysis. (c) Schematic illustration of SIMS depth profiles during in situ liquid SIMS testing. Liquid signals dominate the overall intensity after the SiN membrane was drilled through. Arrow (1) points to the reduced pulse width for a better mass resolution and (d) typical reconstructed SIMS spectrum, showing the signals collected from the liquid.

liquids, as well as liquid−liquid and liquid−solid interfaces, at the molecular level.[46−53] The technique can be considered as a novel molecular "eye" for direct evaluation of various ion clusters and ion−solvent interactions in both nonaqueous and aqueous liquids, providing unique information on molecular structures dominating complex multicomponent solutions. This includes important information on the preferential solvation phenomenon as well as the coordination numbers.[51,52] Importantly, these previous studies demonstrated that in situ liquid SIMS entails a soft ionization process where even weak ion−solvent interactions could be molecularly examined.[54−57] Moreover, the technique is versatile, showing no bias on the detection of positive versus negative ions, and being particularly capable of readily dealing with a wide range of liquid samples including high-concentration, high salty, or relatively viscous sticky samples. Furthermore, compared with traditional mass spectrometric tools, such as electrospray ionization (ESI) MS, in situ liquid SIMS can test high-concentration solutions directly, which allows us to detect the molecular structure of complex liquids in the original status. In situ liquid SIMS is thus perfectly suited to shed light on various important molecular interactions within complex liquids.

Aluminum is the third most abundant element in the earth's crust after oxygen and silicon. Its aqueous chemistry plays an important role in environmental science, geochemistry, medicine, industrial processing, and even nuclear waste treatment.[58−64] For example, the Bayer process that focuses on the crystallization of gibbsite (γ-$Al(OH)_3$, sometimes α-$Al(OH)_3$) from highly concentrated sodium aluminate solutions (always $\geq$ 3 M) is the dominant pathway to produce aluminum materials in large quantities.[65,66] Due to its industrial importance, the exploration of chemical compositions and structures of the aluminum species in Bayer liquors has received wide attention over the past 120 years.[67−69] The dominant species is well known to be the aluminate oxyanion $Al(OH)_4^-$. However, despite the great scientific effort to quantify the existence and structures of various possible polymerized aluminum species that could serve as precursors to gibbsite nucleation, much currently remains a matter of debate and speculation. For instance, the influence of different alkali metal cations on gibbsite nucleation and the regulation of the subsequent aggregation behavior appears to depend in part on the strength of their association with the aluminate anion.[13,70−73] However, the tendency of various cations to form ion pairs with the aluminum species under these highly alkaline conditions remains difficult to unravel due to the generally weak ion-pairing interactions.

Here, we report the molecular characterization of a systematic series of these complex solutions using in situ liquid SIMS, with supporting density functional theory (DFT) calculations, to isolate dominant cluster motifs and help understand their basis in ion-pairing interactions. In particular, by examining both positive and negative secondary-ion signals we provide the first direct molecular-level evidence of preferential formation of Na^+-anion clusters over K^+-anion clusters in mixed Na^+/K^+ alkaline aluminate solutions. DFT calculations are used to assess the veracity of the observed molecular clusters and their solvation characteristics. This work opens a new avenue for understanding complex ion-pairing/solvent interactions using this soft ionization technique.

EXPERIMENTAL SECTION

Sample Preparation. Samples were prepared via dissolving hexagonal-shaped gibbsite nanoplates into NaOH or KOH solutions. The gibbsite nanoplates were synthesized via a previously reported hydrothermal method, and the phase purity and morphologies of gibbsite nanoplates are shown in Figure S1.[74] In a nitrogen glove box, 3.00 g of NaOH (99.99% trace metals basis, Sigma-Aldrich) or 4.21 g of KOH (≥99.95% trace metals basis, Sigma-Aldrich) was dissolved in 4 mL of DI water to form a clear solution in a Teflon liner (20 mL). Then, 2.34 g of gibbsite was added into the NaOH or KOH solution and the Teflon liner was sealed into a Parr steel vessel, which was put into an electric oven equipped with a rotation rack (10 rpm) and held at 80 °C for 12 h. After cooling to room temperature, the final solution was diluted to 3 M (defined as the concentration of aluminate). The final concentration of the Na^+ or K^+ cations was 7.5 M. The Na^+/K^+ 75/25%, Na^+/K^+ 50/50%, and Na^+/K^+ 25/75% samples were prepared via mixing a corresponding portion of 3 M $NaAl(OH)_4$−4.5 M NaOH and 3 M $KAl(OH)_4$−4.5 M KOH fresh solutions. Finally, five representative highly alkaline aluminate solutions named Na^+ 100%, Na^+/K^+ 75/25%, Na^+/K^+ 50/50%, Na^+/K^+ 25/75%, and K^+ 100% were produced for the study.

https://dx.doi.org/10.1021/acs.analchem.0c04070
Anal. Chem. 2021, 93, 1068−1075

Fabrication of the Liquid Cell for ToF-SIMS. The fabrication method of liquid cells can be referred to in our previously published work.[51,52] In short, a silicon frame [5.0 mm (L) × 5.0 mm (W) × 0.2 mm (H)] with a thin silicon nitride membrane (Si_3N_4, 100 nm thickness) was sealed with epoxy glue on the top of a liquid chamber [3.0 mm (L) × 3.0 mm (W) × 0.3 mm (H)], which was premachined on a polyether ether ketone (PEEK) block [3.0 cm (L) × 1.0 cm (W) × 0.6 cm (H)]. After assembling the cell, we injected an interested sample solution (~30 μL) into the liquid chamber through a liquid channel and then sealed the two channel ends. The total volume in the liquid cell is very limited (2−3 μL). Afterward, we fixed the assembled liquid cell onto the sample holder, as shown in Figure 1b, and loaded it into the main chamber of the ToF-SIMS spectrometer for the subsequent in situ SIMS testing.

In Situ Liquid ToF-SIMS Measurements. The in situ liquid SIMS measurements were accomplished using a TOF-SIMS V instrument (ION-TOF GmbH, Münster, Germany). The detailed instrument settings were described in our previous papers.[51,52] In brief, the primary ion beam was a pulsed 25 keV Bi_3^+ at a repetition frequency of 10 kHz, the beam size of which was focused to ~450 nm in diameter. For each measurement, the pulsed Bi_3^+ beam (pulse width = 162.5 ns) was focused on a circular area of ~2 μm in diameter on the SiN membrane to drill an aperture. Once the aperture was created, signal intensities of the species in the solution below the SiN membrane increased sharply. To obtain a better mass resolution, the pulse width was reduced to 62.5 ns when liquid signals became relatively stable (as shown in Figure 1c). The measurement could be stopped when reasonable signal intensities were collected (around 50−200 s). Mass spectra reflecting the solution information were reconstructed from a time region (about 50 s) with stable liquid signals after the pulse width was changed to 62.5 ns. During the measurements, the vacuum pressure in the main chamber was $1-2 \times 10^{-6}$ mbar.

DFT Calculations. All DFT[75] geometry optimization and energy calculations in this study were performed with the molecular Gaussian DFT module implemented in the NWChem software package.[76,77] The Becke three-parameter exchange and Lee−Yang−Parr correlation (B3LYP) functional[78,79] was applied to account for the exchange correlation energy and the 6-311++G(2d,2p) basis set[80,81] was used for all of the elements. The average single bond energy was calculated by the standard energy difference method[82,83] as

$$D(\mathrm{M}-\mathrm{O}) = \frac{1}{m}[E(\mathrm{M}^{n-1}) + nE(\mathrm{A}^-) - E(\mathrm{MA}_n^-)] \quad (1)$$

where D(M−O) is the average single bond energy and $E(\mathrm{M}^{n-1})$, $E(\mathrm{A}^-)$, and $E(\mathrm{M}_n^-)$ are the total energies of the cation M^{n-1}, anion A^-, and anion M_n^-, respectively. m is the number of M−O bonds and n is the stoichiometric number of A^- in M_n^-. For $Na(OH)_2^-$ and $K(OH)_2^-$, M = Na or K, A = OH, and $m = n = 2$. For $Al(OH)_4^-$, M = Al, A = OH, and $m = n = 4$. For $Na(Al(OH)_4)_2^-$ and $K(Al(OH)_4)_2^-$, M = Na or K, A = $Al(OH)_4$, $m = 4$, and $n = 2$ as Na^+ or K^+ forms two bonds with oxygen in each $Al(OH)_4^-$.

RESULTS AND DISCUSSION

We applied in situ liquid ToF-SIMS to obtain direct molecular information on various species comprising our systematic series of five alkaline aluminate solutions (Na^+ 100%, Na^+/K^+ 75/25%, Na^+/K^+ 50/50%, Na^+/K^+ 25/75%, and K^+ 100%) bearing different Na^+/K^+ mixing ratios. A schematic illustration of the technique is shown in Figure 1.

Negative ion spectra of three of the aluminate solutions, including the end-member pure (3 M) sodium aluminate solution and the pure (3 M) potassium aluminate solution and the 1:1 mixed cation case, are shown in Figure 2, and the

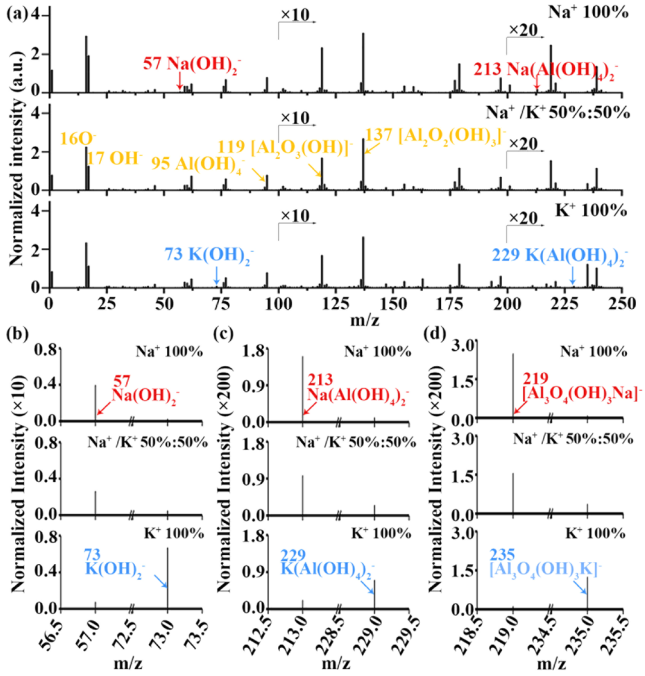

Figure 2. Negative ion spectra of the three representative alkaline aluminate solutions, including Na^+ 100%, Na^+/K^+ 50/50%, and K^+ 100%. (a) m/z range 0−250, (b) comparison of $Na(OH)_2^-$ vs $K(OH)_2^-$, (c) comparison of $Na(Al(OH)_4)_2^-$ vs $K(Al(OH)_4)_2^-$, and (d) comparison of $[Al_3O_4(OH)_3Na]^-$ vs $[Al_3O_4(OH)_3K]^-$. Signal intensities were normalized to the m/z 95 peak intensity, respectively.

negative ion spectra of another two aluminate solutions are given in Figure S2. All of the signal intensities of negative ions were normalized to the signal intensity of $Al(OH)_4^-$ (m/z = 95), respectively. In Figure 2a, the signal intensity of $Al(OH)_4^-$ (m/z = 95) is very clear, consistent with the expectation that this monomeric aluminate anion is a dominant species and a stable structure for these measurements. Alkaline hydroxide ion pairs $Na(OH)_2^-$ (m/z = 57) and $K(OH)_2^-$ (m/z = 73) can also be observed, but their signal intensities are relatively weaker, suggesting that these two structures are less stable, at least much less stable than $Al(OH)_4^-$. In Figure 2b, we found that the ion signal intensity of $[K(OH)_2]^-$ in the pure potassium aluminate solution is 1.7 times as high as that of $[Na(OH)_2]^-$ in the pure sodium aluminate solution. Such a slight difference may be attributed to slight differences of sputter yields and ionization yields for these two species. By contrast, the intensity of $[Na(OH)_2]^-$ in the 1:1 (Na/K = 1:1) mixed alkaline aluminate solution becomes 6.4 times as high as that of $[K(OH)_2]^-$, which provides solid molecular evidence that the Na^+-OH^- interaction is undoubtedly stronger than the K^+-OH^- interaction. Moreover, as shown in Figure 2c, the normalized signal intensity of $[Na(Al(OH)_4)_2]^-$ (m/z = 213) in the pure sodium aluminate solution is 1.3 times higher than that of $[K(Al(OH)_4)_2]^-$ (m/z = 229) in the pure potassium aluminate solution. Whereas, in the 1:1 (Na/K = 1:1) mixed

https://dx.doi.org/10.1021/acs.analchem.0c04070
Anal. Chem. 2021, 93, 1068−1075

solution the difference increased up to 3.2 times, which reveals the preferential interaction between Na^+ and $Al(OH)_4^-$ compared to that between K^+ and $Al(OH)_4^-$. Similarly, the normalized signal intensity of $[Al_3O_4(OH)_3Na]^-$ (m/z = 219) in the pure sodium aluminate solution is twice as high as that of $[Al_3O_4(OH)_3K]^-$ (m/z = 235) in the pure potassium aluminate solution (Figure 2d). In the case of the 1:1 mixed alkaline aluminate solution, the $[Al_3O_4(OH)_3Na]^-$ ion shows a distinctly higher signal intensity, which is 3.6 times higher than that of the $[Al_3O_4(OH)_3K]^-$, further confirming the stronger Na^+-anion interaction than the K^+-anion interaction. A comparison of the normalized signal intensities of different negative ion pairs is given in Table S1.

Such findings are qualitatively consistent with previously reported results. For example, various techniques, including Raman spectroscopy,[84−87] IR,[86] NMR,[85,88−90] solution XRD,[33] and quasi-elastic neutron scattering (QENS),[3,90] have demonstrated the stable $Al(OH)_4^-$ species in alkaline aluminate solutions,[87] and furthermore it has been suggested that Na^+ exhibits a stronger ion-pairing ability with the available anions such as $Al(OH)_4^-$ and OH^-, than K^+.[3,35,36,67,85,91,92] But compared to these traditionally used tools, a unique strength of our in situ liquid SIMS approach is direct molecular recognition, enabling a direct proof of the preferential affinity of Na^+ over K^+ in mixed solutions. Few other tools can provide such information. For example, the combination of QENS and proton-pulsed field gradient-NMR (^{1}H PFG-NMR) measurements suggested the formation of the alkali metal hydroxide/aluminate ion pairs via probing the dynamics of water and the aluminum species, also indicating that the ion-pair formation in sodium-based aluminate solutions was much more facile than in potassium-based solutions.[3,33,90] But the collection, analysis, and fitting of such data are cumbersome and not without ambiguities for complex compositions in which a series of ion pairs, aluminum-based monomers, dimers, trimers, and even large oligomers may be present.[3,33,35,40,67,85,87,90,93] It is furthermore noteworthy that such approaches only allow inference of the formation of ion-pairs, without showing directly that they exist. In contrast, in SIMS spectra, accurate m/z values facilitate easy assignment of different ion cluster species, e.g., $[Na(Al(OH)_4)_2]^-$ at m/z 213 and $[K(Al(OH)_4)_2]^-$ at m/z 229, from the Na^+ and K^+ mixed aluminate solutions, and make a direct comparison available. In principle, it is also possible to compare the affinity of different anions with the same cation in a mixed solution. Thus, the in situ liquid ToF-SIMS approach brings a new value to investigating complex molecular structures of species and ion interactions in alkaline aluminate solutions.

Figure 3 shows the positive ion spectra from the same three solutions shown in Figure 2 and the positive ion spectra of another two aluminate solutions are given in Figure S3. From examination of the two end-member compositions, one can see the Na^+ (m/z = 23) and K^+ (m/z = 39) domination of the respective spectra, evidence of the high ionization yields of these two ions in aluminate solutions. The positive spectrum of the 100% sodium aluminate solution (Figure 3a) shows clear Na^+-anion cluster peaks such as $[Na_2(OH)]^+$ (m/z = 63) and $[Na_2(Al(OH))_4]^+$ (m/z = 141) and the spectrum of the 100% potassium aluminate solution (Figure 3c) shows clear K^+-anion cluster peaks such as $[K_2(OH)]^+$ (m/z = 95) and $[K_2(Al(OH))_4]^+$ (m/z = 173), which indicate such species are stable structures. It was found that the signal intensity of $[K_2(OH)]^+$ (m/z = 95) in the pure potassium aluminate solution is 1.89

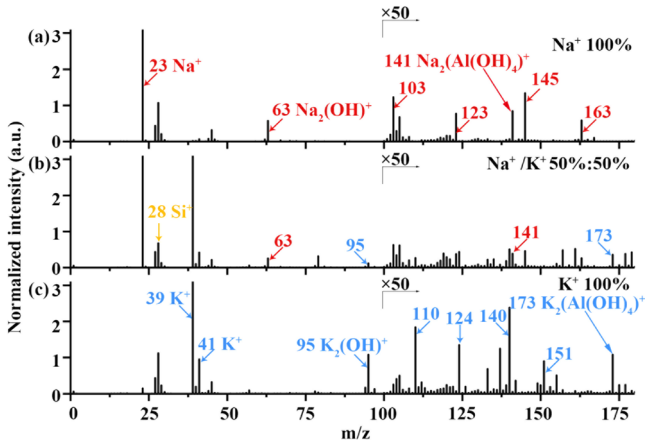

Figure 3. Positive ion spectra (m/z range 0−180) of the three representative alkaline aluminate solutions, including Na^+100%, Na^+/K^+ 50/50%, and K^+100%. Signal intensities were normalized to the m/z 27 (Al^+) peak intensity. In the 100% Na^+ spectrum, the red arrows point to ions such as $[Na_3(OH)_2]^+$ (m/z 103), $[AlO(OH)_2Na_2]^+$ (m/z 123), $[AlO_3HNa_3]^+$ (m/z 145), and $[AlO_3HNa_3\cdot H_2O]^+$ (m/z 163). In the 100% K^+ spectrum, the blue arrows point to ions such as $[K_2O_2]^+$ (m/z 110), $[K_2NO_2]^+$ (m/z 124), $[K_2AlO_2]^+$ (m/z 137), $[K_2NO_3]^+$ (m/z 140), and $[K_3(OH)_2]^+$ (m/z 151).

times as high as that of $[Na_2(OH)]^+$ (m/z = 63) in the pure sodium aluminate solution. Although one might initially suspect that the sputter yield and ionization yield of $[Na_2(OH)]^+$ may be lower than those of $[K_2(OH)]^+$, the signal intensities of Na^+-anion clusters in the mixed solution (Figure 3b) are higher than those of the corresponding K^+-anion species. For instance, the normalized signal intensity of $[Na_2(OH)]^+$ (m/z = 63) is 2.1 times higher than that of $[K_2(OH)]^+$ (m/z = 95) in the 1:1 mixed alkaline aluminate solution, as shown in Figure 3b. Meanwhile, the ion signal intensity of the $[Na_2(Al(OH))_4]^+$ (m/z = 141) peak is 8% larger than that of the $[K_2(Al(OH))_4]^+$ (m/z = 173) peak, which also illustrates stronger Na^+-anion interactions in the mixed alkaline aluminate solutions. A comparison of the normalized signal intensities of different positive ion pairs is given in Table S2.

Quantitative comparison of Na^+-anion interactions with K^+-anion interactions is of great interest. However, absolute quantification using SIMS is problematic because different ion species may have different sputter yields and/or ionization yields (so−called "matrixed effect"). Fortunately, useful semiquantitative information can be obtained based on normalization because it minimizes the differences of sputter and/or ionization yields. Figure 4 shows a summary of the semiquantitative comparison of Na^+-anion interactions with K^+-anion interactions, and the normalization details are given in the Supporting Information. Figure 4a shows the relative signal intensities of $Na(OH)_2^-$ in alkaline aluminate solutions at different mixed ratios. The ideal values of the relative $Na(OH)_2^-$ signal intensity in 25, 50, and 75% Na alkaline aluminate solutions should be 0.25, 0.5, and 0.75, respectively. If no preferential effect occurs, Na^+ ions and K^+ ions should have the same opportunities to associate with hydroxide ions, and the proportion of the Na^+-hydroxide ion species should be the same as these ideal values. But the actual measured data reveal significantly larger values, at 0.59, 0.86, and 0.95 in the corresponding solutions, indicating an obvious preferential behavior in the combination of sodium ions and hydroxide

https://dx.doi.org/10.1021/acs.analchem.0c04070
Anal. Chem. 2021, 93, 1068−1075

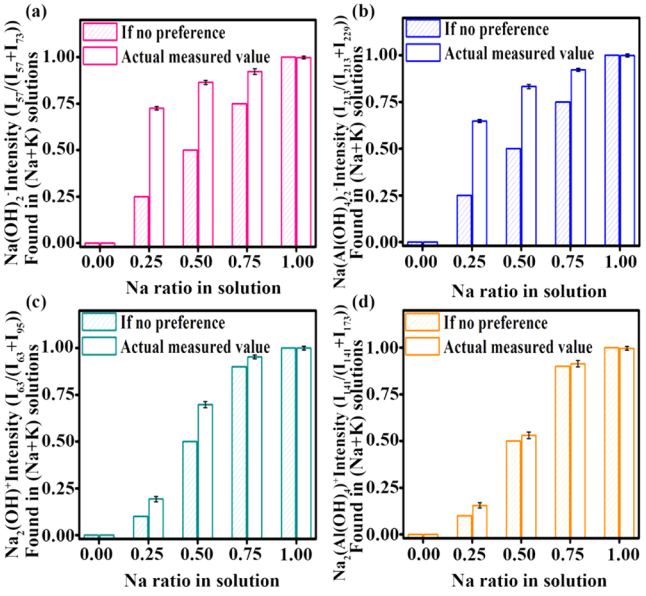

Figure 4. Comparison of the relative signal intensities of ideal and actual measured values in alkaline aluminate solutions at different mixed ratios. (a) $Na(OH)_2^-$ vs $K(OH)_2^-$, (b) $Na(Al(OH)_4)_2^-$ vs $K(Al(OH)_4)_2^-$, (c) $Na_2(OH)^+$ vs $K_2(OH)^+$, and (d) $Na_2(Al(OH)_4)^+$ vs $K_2(Al(OH)_4)^+$.

ions. Similarly, as shown in Figure 4b, the ideal values of the relative $Na(Al(OH)_4)_2^-$ signal intensity at different mixed ratios of 25, 50, and 75% should be 0.25, 0.50, and 0.75, while the actual measured relative signal intensities are 0.61, 0.88, and 0.98, respectively. All of the above results strongly suggest that the Na^+-aluminate anion interactions are much stronger than the corresponding K^+-aluminate anion interactions. Figure 4c depicts the relative signal intensities of $Na_2(OH)^+$ in alkaline aluminate solutions at different mixed ratios from the positive ion spectra. At 25, 50, and 75% Na, the actual measured relative $Na_2(OH)^+$ signal intensities are 0.19, 0.70, and 0.95, respectively, which are larger than those of the corresponding ideal values of 0.10, 0.50, and 0.90 (because of two Na^+), also reflecting the preferential Na^+-anion interactions over K^+-anion interactions. In addition, the relative signal intensities of $Na_2(Al(OH)_4)^+$ in alkaline aluminate solutions at different mixed ratios of 25, 50, and 75% Na are 0.16, 0.53, and 0.91, respectively, as shown in Figure 4d. Although we found that these measured data were slightly larger than the corresponding ideal values of 0.1, 0.5, and 0.9, they still suggest the preferential Na^+-anion interactions over K^+-anion interactions.

To evaluate the compositional and structural stabilities of some of these key clusters, we performed DFT total energy minimization on cluster ions in the vacuum. Figures 5 and S4 show the resulting structures of major anion types indicated by the SIMS measurements, with the corresponding bond energies of the Na and K compounds given in Tables 1 and S3. Comparison of the values shows that the average Al−O bond energy is much higher than Na−O and K−O bond energies in hydroxyl compounds. This reveals clearly that Al^{3+} forms a stronger bond with OH^- than Na^+ and K^+, confirming expectations that $Al(OH)_4^-$ is a relatively more stable structure. Furthermore, the calculations also show that the Na−O bond energy is higher than the K−O bond energy in both hydroxyl and aluminate compounds, suggesting that the interactions

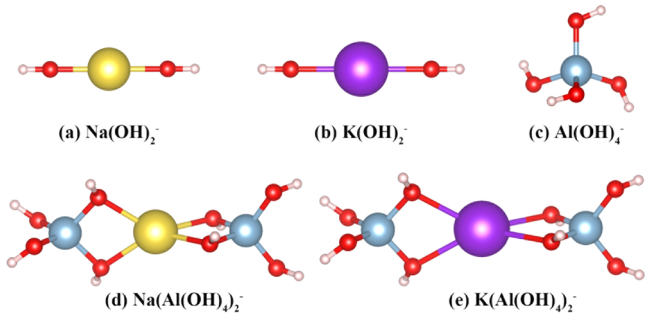

Figure 5. Structures of the five anions in this work presented in the ball-and-stick form, which are (a) $Na(OH)_2^-$, (b) $K(OH)_2^-$, (c) $Al(OH)_4^-$, (d) $Na(Al(OH)_4)_2^-$, and (e) $K(Al(OH)_4)_2^-$. Color key: Na = yellow, K = purple, Al = blue, O = red, and H = white.

Table 1. Bond Energies of Na and K Compounds

bond	average bond energy (kJ/mol)
Al−O in $Al(OH)_4^-$	1610.14
Na−O in $Na(OH)_2^-$	456.50
K−O in $K(OH)_2^-$	398.89
Na−O in $Na(Al(OH)_4)_2^-$	191.97
K−O in $K(Al(OH)_4)_2^-$	166.53

between Na^+ and anions should be stronger than those between K^+ and the corresponding anions, consistent with the evidence collected by SIMS measurements. In addition to supporting the observed cluster types and trends, the theory/experiment agreement reinforces the applicability of the in situ liquid ToF-SIMS technique itself.

The computed energetics can be further used to address some of the weaker associations indicated from the SIMS data. For example, from Table 1, we can estimate the ΔG of the reaction of $Na^+ + [K(OH)_2]^- \Leftrightarrow K^+ + [Na(OH)_2]^-$ in the vacuum, which is about −115 kJ/mol. If we suppose Na^+ and K^+ have a similar concentration, based on the SIMS measurement result of $[Na(OH)_2]^-/[K(OH)_2]^- \approx 7$ in the 50/50% sample, shown in Figure 4, and the equation $-\Delta G = R{\cdot}T{\cdot}\mathrm{Ln}(k)$, the RT in the in situ liquid SIMS measurement is calculated to be 60 kJ/mol, which can be regarded as the disturbance intensity of sputtering and ionization processes in the in situ liquid SIMS measurement. It should be noted that, in aqueous environments, the absolute value of the ΔG can be 25% lower due to solvation effects (see the Supporting Information for more details). Moreover, due to the preferential association of Na^+ with anions, the free Na^+ in solution should be less than the free K^+. If so, the RT value in real conditions should be no more than 40−50 kJ/mol (about 0.5 eV). This value is comparable with the vaporization heat of water (~40 kJ/mol), and significantly lower than the energy of general chemical bonds (several hundred kJ/mol, or a few eV). Therefore, the result confirms that in situ liquid SIMS is a soft ionization technique, and it can be used to study weak interactions within liquids on a molecular level.

In our previous work, in situ liquid SIMS was used to study another kind of weak interaction, namely, the ion−solvent interaction, in aqueous environments,[51,52] the energy level of which is 20−40 kJ/mol.[52] This energy value is lower than our estimated disturbance intensity (RT, 40−50 kJ/mol) in the present study. Such a difference can be attributed to the fact that the disturbance intensity is an average value, and the case-to-case distribution can vary within a wide range. Therefore,

https://dx.doi.org/10.1021/acs.analchem.0c04070
Anal. Chem. 2021, 93, 1068−1075

some interactions that are slightly weaker than the energy level of the disturbance intensity can still persist in the mass spectrometric analysis using in situ liquid SIMS.

The implications of our collective new findings for these complex alkaline aluminate solutions are broadly relevant across material synthesis, separation, environmental conservation, pharmaceutical preparations, analysis, and so on.[1−7] Next step, we will probe critical saturation states for multinuclear Al clusters that are present incipient to and during precipitation in the highly alkaline systems. They include in particular Bayer liquors, as well as legacy nuclear wastes stored in hundreds of tanks at the Hanford Site (WA), the Savannah River Site (SC), and the West Valley Nuclear Site (NY).[13,61,94,95] In these systems, ion-pair formation and the ion-pairing ability of counterions in these multicomponent solutions are key governing factors for crystallization, in particular with respect to controlling the stability and lifetime of electrolyte solutions in terms of the precipitation rate, and also the crystalline phase of resulting nanoparticles.[3,6,12] However, the intrinsic nature of multicomponents makes the traditional analysis tools, such as NMR, IR, Raman, and those X-ray-related tools, less useful due to the lack of molecular recognition capability. The direct molecular evidence of formation of Na^+/K^+-anion clusters detected by in situ liquid SIMS could ultimately help determine a basis for understanding prenucleation cluster dynamics and thus controlling the crystallization behavior of gibbsite in alkaline aluminate solutions. More broadly, the in situ liquid SIMS technique could be used to explore the ion-pairing ability of rare earth ions or organic molecules such as peptides and proteins with different ionic liquids or additives that may facilitate the advancement of separation approaches to purify the rare earth elements or pharmaceuticals.[2,8−11,21] Moreover, understanding ion-pair formation between organic ligands and metal ions, alkaline ions and organic species, Pb(II) and halide ions, and charged electrolyte species and counterions in flow batteries may provide insights into the development of novel metal−organic frameworks (MOFs), perovskites, battery materials for energy storage, environment, and catalysis.[96−99]

CONCLUSIONS

In summary, in situ liquid ToF-SIMS was successfully applied to investigate ion pairing including weak interactions in alkaline multicomponent aluminate solutions with direct molecular information on key ion clusters. A series of Na^+-anion and K^+-anion species could be clearly observed and distinguished in the spectra, with the corresponding signal intensities of Na^+-aluminate clusters and the corresponding K^+-aluminate clusters in both positive ion spectra and negative ion spectra that provide direct molecular proof of the preferential interaction of Na^+ over K^+ with aluminate anions. The key clusters and their relative energetics were verified by DFT calculations, which showed that the energy difference between the interested Na^+-clusters and the corresponding K^+ -clusters is about 100−120 kJ/mol, consistent with the ability of SIMS to easily differentiate these clusters on that basis. More interestingly, the combination of in situ SIMS data and DFT calculation data suggests that the disturbance intensity during sputtering and ionization processes in these systems is around 40−50 kJ/mol, being significantly lower than the energy of general chemical bonds. The collective findings reinforce the utility of in situ liquid ToF-SIMS as a powerful tool to explore complex interactions, such as ion-pair competition, ion−solvent interactions, as well as many other types of weak interactions, in liquid environments, particularly when combined with molecular computations.

ASSOCIATED CONTENT

Supporting Information

The Supporting Information is available free of charge at https://pubs.acs.org/doi/10.1021/acs.analchem.0c04070.

SEM and XRD images of gibbsite; negative and positive ion spectra of Na^+/K^+ 75/25% and Na^+/K^+ 25/75% alkaline aluminate solutions; structures of $Al_3O_4(OH)_3^{2-}$, $[Al_3O_4(OH)_3Na]^-$, and $[Al_3O_4(OH)_3K]^-$; tables of signal intensities of important peaks in the negative or positive spectra and calculated bond energies of Na and K compounds; and relative signal intensity normalized details (PDF)

AUTHOR INFORMATION

Corresponding Authors

Junwu Zhu − *Nanjing University of Science and Technology, Nanjing 210094, China;* orcid.org/0000-0002-7518-9683; Email: zhujw@njust.edu.cn

Kevin M. Rosso − *Pacific Northwest National Laboratory, Richland, Washington 99354, United States;* orcid.org/0000-0002-8474-7720; Email: kevin.rosso@pnnl.gov

Zihua Zhu − *Pacific Northwest National Laboratory, Richland, Washington 99354, United States;* orcid.org/0000-0001-5770-8462; Email: zihua.zhu@pnnl.gov

Xin Zhang − *Pacific Northwest National Laboratory, Richland, Washington 99354, United States;* orcid.org/0000-0003-2000-858X; Email: xin.zhang@pnnl.gov

Authors

Yining Wang − *Nanjing University of Science and Technology, Nanjing 210094, China; Pacific Northwest National Laboratory, Richland, Washington 99354, United States*

Duo Song − *Pacific Northwest National Laboratory, Richland, Washington 99354, United States*

Yadong Zhou − *Pacific Northwest National Laboratory, Richland, Washington 99354, United States*

Cuixia Cheng − *Pacific Northwest National Laboratory, Richland, Washington 99354, United States*

Yanyan Zhang − *Institute of Chemistry, Chinese Academy of Sciences, Beijing 100190, China;* orcid.org/0000-0002-2048-145X

Carolyn I. Pearce − *Pacific Northwest National Laboratory, Richland, Washington 99354, United States;* orcid.org/0000-0003-3098-1615

Zheming Wang − *Pacific Northwest National Laboratory, Richland, Washington 99354, United States*

Sue B. Clark − *Pacific Northwest National Laboratory, Richland, Washington 99354, United States*

Complete contact information is available at: https://pubs.acs.org/10.1021/acs.analchem.0c04070

Author Contributions

All authors have given approval to the final version of the manuscript.

Notes

The authors declare no competing financial interest.

https://dx.doi.org/10.1021/acs.analchem.0c04070
Anal. Chem. 2021, 93, 1068−1075

■ ACKNOWLEDGMENTS

This research was supported by IDREAM (Interfacial Dynamics in Radioactive Environments and Materials), an Energy Frontier Research Center funded by the U.S. Department of Energy (DOE), Office of Science, Basic Energy Sciences (BES). A portion of this research was performed in the Environmental Molecular Sciences Laboratory (EMSL), a national scientific user facility sponsored by the DOE Office of Biological and Environmental Research and located at PNNL. PNNL is a multiprogram national laboratory operated for DOE by Battelle Memorial Institute under Contract DE-AC05-76RL0-1830. Y.W. acknowledges support from the China Scholarship Council (CSC) for the financial support during her studies in the United States.

■ REFERENCES

(1) Marcus, Y. H. G. *Chem. Rev.* **2006**, *106*, 4585−4621.
(2) Quintanar-Guerrero, D.; Allémann, E.; Fessi, H.; Doelker, E. *Pharm. Res.* **1997**, *14*, 119−127.
(3) Wang, H. W.; Graham, T. R.; Mamontov, E.; Page, K.; Stack, A. G.; Pearce, C. I. *J. Phys. Chem. Lett.* **2019**, *10*, 3318−3325.
(4) Oda, R.; Huc, I.; Schmutz, M.; Candau, S. J.; MacKintosh, F. C. *Nature* **1999**, *399*, 566−569.
(5) Barthou, C.; Barthem, R. B. *J. Lumin.* **1990**, *46*, 9−15.
(6) Jiang, G.; Fu, H.; Savino, K.; Qian, J.; Wu, Z.; Guan, B. *Cryst. Growth Des.* **2013**, *13*, 5128−5134.
(7) Stahl, N. G.; Zuccaccia, C.; Jensen, T. R.; Marks, T. J. *J. Am. Chem. Soc.* **2003**, *125*, 5256−5257.
(8) Boardman, N. K.; Partridge, S. M. *Nature* **1953**, *171*, 208−210.
(9) Nagy, G.; Kedia, K.; Attah, I. K.; Garimella, S. V. B.; Ibrahim, Y. M.; Petyuk, V. A.; Smith, R. D. *Anal. Chem.* **2019**, *91*, 4374−4380.
(10) Vazdar, M.; Heyda, J.; Mason, P. E.; Tesei, G.; Allolio, C.; Lund, M.; Jungwirth, P. *Acc. Chem. Res.* **2018**, *51*, 1455−1464.
(11) Fahim, A.; Annunziata, O. *Langmuir* **2020**, *36*, 2635−2643.
(12) Boyle, D. S.; Govender, K.; O'Brien, P. *Chem. Commun.* **2002**, 80−81.
(13) Li, Z.; Liu, G.; Li, X.; Qi, T.; Peng, Z.; Zhou, Q. *Cryst. Growth Des.* **2019**, *19*, 1778−1785.
(14) Koutmou, K. S.; Casiano-Negroni, A.; Getz, M. M.; Pazicni, S.; Andrews, A. J.; Penner-Hahn, J. E.; Al-Hashimi, H. M.; Fierke, C. A. *Proc. Natl. Acad. Sci. U.S.A.* **2010**, *107*, 2479−2484.
(15) Reddy, G. N.; Ballesteros-Garrido, M.; Lacour, R.; Caldarelli, J. *Angew. Chem., Int. Ed.* **2013**, *125*, 3337−3340.
(16) Nakamura, K.; Hirota, N. *Chem. Phys. Lett.* **1969**, *3*, 137−139.
(17) Lü, J. M.; Rosokha, S. V.; Neretin, I. S.; Kochi, J. K. *J. Am. Chem. Soc.* **2006**, *128*, 16708−16719.
(18) Chao, C. C.; Lunsford, J. H. *J. Chem. Phys.* **1972**, *57*, 2890−2898.
(19) Ault, B. S.; Andrews, L. *Inorg. Chem.* **1977**, *16*, 2024−2028.
(20) Moskovits, M.; Michaelian, K. H. *J. Am. Chem. Soc.* **1980**, *102*, 2209−2215.
(21) Rudolph, W. W.; Irmer, G. *Dalton Trans.* **2017**, *46*, 4235−4244.
(22) Brandes, E.; Stage, C.; Motschmann, H.; Rieder, J.; Buchner, R. *J. Chem. Phys.* **2014**, *141*, No. 18C509.
(23) van der Post, S. T.; Hunger, J.; Bonn, M.; Bakker, H. J. *J. Phys. Chem. B* **2014**, *118*, 4397−4403.
(24) Streubel, S.; Schulze-Zachau, F.; Weissenborn, E.; Braunschweig, B. *J. Phys. Chem. C* **2017**, *121*, 27992−28000.
(25) Sipos, P.; May, P.; Heffer, G.; Kron, I. *J. Chem. Soc., Chem. Commun.* **1994**, 2355−2356.
(26) de Silva, A. P.; McClean, G. D.; Pagliari, S. *Chem. Commun.* **2003**, 2010−2011.
(27) Sthoer, A.; Hladilkova, J.; Lund, M.; Tyrode, E. *Phys. Chem. Chem. Phys.* **2019**, *21*, 11329−11344.
(28) Wachter, W.; Fernandez, S.; Buchner, R.; Hefter, G. *J. Phys. Chem. B* **2007**, *111*, 9010−9017.
(29) Uejio, J. S.; Schwartz, C. P.; Duffin, A. M.; Drisdell, W. S.; Cohen, R. C.; Saykally, R. J. *Proc. Natl. Acad. Sci. U.S.A.* **2008**, *105*, 6809−6812.
(30) Carlier, D.; Cheng, J.-H.; Pan, C.-J.; Ménétrier, M.; Delmas, C.; Hwang, B.-J. *J. Phys. Chem. C* **2013**, *117*, 26493−26500.
(31) Simonet, V.; Calzavara, Y.; Hazemann, J. L.; Argoud, R.; Geaymond, O.; Raoux, D. *J. Chem. Phys.* **2002**, *117*, 2771−2781.
(32) Takahashi, R.; Narayanan, T.; Sato, T. *J. Phys. Chem. Lett.* **2017**, *8*, 737−741.
(33) Radnai, T.; May, P. M.; Hefter, G. T.; Sipos, P. *J. Phys. Chem. A* **1998**, *102*, 7841−7850.
(34) León, C.; Lucía, M. L.; Santamaría, J.; París, M. A.; Sanz, J.; Várez, A. *Phys. Rev. B* **1996**, *54*, 184−189.
(35) Sipos, P.; Schibeci, M.; Peintler, G.; May, P. M.; Hefter, G. *Dalton Trans.* **2006**, 1858−1866.
(36) Li, J.; Prestidge, C. A.; Addai-Mensah, J. *J. Chem. Eng. Data* **2000**, *45*, 665−671.
(37) Gerson, A. R.; Ralston, J.; Smart, R. S. C. *Colloids Surf., A* **1996**, *110*, 105−117.
(38) Hattori, T.; Saito, T.; Ishida, K.; Scheinost, A. C.; Tsuneda, T.; Nagasaki, S.; Tanaka, S. *Geochim. Cosmochim. Acta* **2009**, *73*, 5975−5988.
(39) White, C. E.; Provis, J. L.; Kearley, G. J.; Riley, D. P.; van Deventer, J. S. *Dalton Trans.* **2011**, *40*, 1348−1355.
(40) Pouvreau, M.; Dembowski, M.; Clark, S. B.; Reynolds, J. G.; Rosso, K. M.; Schenter, G. K.; Pearce, C. I.; Clark, A. E. *J. Phys. Chem. B* **2018**, *122*, 7394−7402.
(41) Guo, J.; Liu, S.; Wang, Z.; Cao, J.; Wang, D. *Chem. Phys. Lett.* **2020**, *739*, No. 136979.
(42) Guo, J.; Wang, Z.; Cao, J.; Gong, X. *J. Mol. Struct.* **2020**, *1199*, No. 126791.
(43) Drexler, C. I.; Miller, T. C.; Rogers, B. A.; Li, Y. C.; Daly, C. A., Jr.; Yang, T.; Corcelli, S. A.; Cremer, P. S. *J. Am. Chem. Soc.* **2019**, *141*, 6930−6936.
(44) Roy, S.; Baer, M. D.; Mundy, C. J.; Schenter, G. K. *J. Chem. Theory Comput.* **2017**, *13*, 3470−3477.
(45) Watling, H.; Fleming, S.; Bronswijk, W.; Rohl, A. *J. Chem. Soc., Dalton Trans.* **1998**, 3911−3918.
(46) Yang, L.; Yu, X.-Y.; Zhu, Z.; Iedema, M. J.; Cowin, J. P. *Lab Chip* **2011**, *11*, 2481−2484.
(47) Hua, X.; Yu, X.-Y.; Wang, Z.; Yang, L.; Liu, B.; Zhu, Z.; Tucker, A. E.; Chrisler, W. B.; Hill, E. A.; Thevuthasan, T.; Lin, Y.; Liu, S.; Marshall, M. J. *Analyst* **2014**, *139*, 1609−1613.
(48) Zhu, Z.; Zhou, Y.; Yan, P.; Vemuri, R. S.; Xu, W.; Zhao, R.; Wang, X.; Thevuthasan, S.; Baer, D. R.; Wang, C.-M. *Nano Lett.* **2015**, *15*, 6170−6176.
(49) Yu, J.; Zhou, Y.; Hua, X.; Liu, S.; Zhu, Z.; Yu, X.-Y. *Chem. Commun.* **2016**, *52*, 10952−10955.
(50) Wang, Z.; Zhang, Y.; Liu, B.; Wu, K.; Thevuthasan, S.; Baer, D. R.; Zhu, Z.; Yu, X.-Y.; Wang, F. *Anal. Chem.* **2017**, *89*, 960−965.
(51) Zhang, Y.; Su, M.; Yu, X.; Zhou, Y.; Wang, J.; Cao, R.; Xu, W.; Wang, C.; Baer, D. R.; Borodin, O.; Xu, K.; Wang, Y.; Wang, X.-L.; Xu, Z.; Wang, F.; Zhu, Z. *Anal. Chem.* **2018**, *90*, 3341−3348.
(52) Zhang, Y.; Zeng, W.; Huang, L.; Liu, W.; Jia, E.; Zhao, Y.; Wang, F.; Zhu, Z. *Anal. Chem.* **2019**, *91*, 7039−7046.
(53) Zhang, Y.; Wang, J.-G.; Yu, X.; Baer, D. R.; Zhao, Y.; Mao, L.; Wang, F.; Zhu, Z. *ACS Energy Lett.* **2019**, *4*, 215−221.
(54) Lu, S.-M.; Peng, Y.-Y.; Ying, Y.-L.; Long, Y.-T. *Anal. Chem.* **2020**, *92*, 5621−5644.
(55) Liu, Y.-Y.; Zhang, S.-Z.; Ying, Y.-L.; Xia, H.-L.; Hua, X.; Long, Y.-T. *J. Phys. Chem. Lett.* **2019**, *10*, 4935−4941.
(56) Hua, X.; Xia, H.-L.; Long, Y.-T. *Chem. Sci.* **2019**, *10*, 6215−6219.
(57) Hua, X.; Li, H.-W.; Long, Y.-T. *Anal. Chem.* **2018**, *90*, 1072−1076.
(58) Swaddle, T. W.; Rosenqvist, J.; Yu, P.; Bylaska, E.; Phillips, B. L.; Casey, W. H. *Science* **2005**, *308*, 1450−1453.
(59) Furrer, G.; Phillips, B. L.; Ulrich, K.-U.; Pöthig, R.; Casey, W. H. *Science* **2002**, *297*, 2245−2247.

https://dx.doi.org/10.1021/acs.analchem.0c04070
Anal. Chem. 2021, 93, 1068−1075

(60) Cui, W.; Zhang, X.; Pearce, C. I.; Chen, Y.; Zhang, S.; Liu, W.; Engelhard, M. H.; Kovarik, L.; Zong, M.; Zhang, H.; Walter, E. D.; Zhu, Z.; Heald, S. M.; Prange, M. P.; De Yoreo, J. J.; Zheng, S.; Zhang, Y.; Clark, S. B.; Li, P.; Wang, Z.; et al. *Environ. Sci. Technol.* **2019**, *53*, 11043−11055.
(61) Peterson, R. A.; Buck, E. C.; Chun, J.; Daniel, R. C.; Herting, D. L.; Ilton, E. S.; Lumetta, G. J.; Clark, S. B. *Environ. Sci. Technol.* **2018**, *52*, 381−396.
(62) Zhang, X.; Cui, W.; Hu, J. Z.; Wang, H.-W.; Prange, M. P.; Wan, C.; Jaegers, N. R.; Zong, M.; Zhang, H.; Pearce, C. I.; Li, P.; Wang, Z.; Clark, S. B.; Rosso, K. M. *Cryst. Growth Des.* **2019**, *19*, 5557−5567.
(63) Zhang, X.; Cui, W.; Page, K. L.; Pearce, C. I.; Bowden, M. E.; Graham, T. R.; Shen, Z.; Li, P.; Wang, Z.; Kerisit, S.; N'Diaye, A. T.; Clark, S. B.; Rosso, K. M. *Cryst. Growth Des.* **2018**, *18*, 3596−3606.
(64) Zhang, X.; Huestis, P. L.; Pearce, C. I.; Hu, J. Z.; Page, K.; Anovitz, L. M.; Aleksandrov, A. B.; Prange, M. P.; Kerisit, S.; Bowden, M. E.; Cui, W.; Wang, Z.; Jaegers, N. R.; Graham, T. R.; Dembowski, M.; Wang, H.-W.; Liu, J.; N'Diaye, A. T.; Bleuel, M.; Mildner, D. F. R.; et al. *ACS Appl. Nano Mater.* **2018**, *1*, 7115−7128.
(65) Zhang, R.; Zheng, S.; Ma, S.; Zhang, Y. *J. Hazard. Mater.* **2011**, *189*, 827−835.
(66) Yu, Z.; Chen, Y.; Niu, Y.; Tang, Y.; Wan, P.; Lv, Z.; Yang, X. J. *Angew. Chem., Int. Ed.* **2011**, *50*, 11719−11723.
(67) Sipos, P. *J. Mol. Liq.* **2009**, *146*, 1−14.
(68) Li, X.; Wang, D.; Zhou, Q.; Liu, G.; Peng, Z. *Hydrometallurgy* **2011**, *106*, 93−98.
(69) Li, J.; Yin, Z.; Ding, Z.; Liu, W.; Wei, T.; Chen, Q.; Zhang, W. *Hydrometallurgy* **2016**, *163*, 77−82.
(70) Addai-Mensah, J.; Ralston, J. *J. Colloid Interface Sci.* **1999**, *215*, 124−130.
(71) Li, J.; Prestidge, C. A.; Addai-Mensah, J. *J. Cryst. Growth* **2000**, *219*, 451−464.
(72) Li, J.; Prestidge, C. A.; Addai-Mensah, J. *J. Colloid Interface Sci.* **2000**, *224*, 317−324.
(73) Prestidge, C. A.; Ametov, I. *J. Cryst. Growth* **2000**, *209*, 924−933.
(74) Zhang, X.; Zhang, X.; Graham, T. R.; Pearce, C. I.; Mehdi, B. L.; N'Diaye, A. T.; Kerisit, S.; Browning, N. D.; Clark, S. B.; Rosso, K. M. *Cryst. Growth Des.* **2017**, *17*, 6801−6808.
(75) Becke, A. D. *J. Chem. Phys.* **2014**, *140*, No. 18A301.
(76) Valiev, M.; Bylaska, E. J.; Govind, N.; Kowalski, K.; Straatsma, T. P.; Van Dam, H. J. J.; Wang, D.; Nieplocha, J.; Apra, E.; Windus, T. L.; de Jong, W. A. *Comput. Phys. Commun.* **2010**, *181*, 1477−1489.
(77) Aprà, E.; Bylaska, E. J.; de Jong, W. A.; Govind, N.; Kowalski, K.; Straatsma, T. P.; Valiev, M.; van Dam, H. J. J.; Alexeev, Y.; Anchell, J.; Anisimov, V.; Aquino, F. W.; Atta-Fynn, R.; Autschbach, J.; Bauman, N. P.; Becca, J. C.; Bernholdt, D. E.; Bhaskaran-Nair, K.; Bogatko, S.; Borowski, P.; et al. *J. Chem. Phys.* **2020**, *152*, No. 184102.
(78) Becke, A. D. *J. Chem. Phys.* **1993**, *98*, 5648−5652.
(79) Lee, C.; Yang, W.; Parr, R. *J. Phys. Rev. B* **1988**, *37*, 785−789.
(80) Davidson, E. R.; Feller, D. *Chem. Rev.* **1986**, *86*, 681−696.
(81) Hehre, W. *Ab initio Molecular Orbital Theory*; Wiley: New York, 1986.
(82) Scheiner, S. *Hydrogen Bonding: A Theoretical Perspective*; Oxford University Press on Demand, 1997.
(83) Boys, S. F.; Bernardi, F. *Mol. Phys.* **1970**, *19*, 553−556.
(84) Johnston, C. T.; Agnew, S. F.; Schoonover, J. R.; Kenney, J. W.; Page, B.; Osborn, J.; Corbin, R. *Environ. Sci. Technol.* **2002**, *36*, 2451−2458.
(85) Sipos, P.; Hefter, G.; May, P. M. *Talanta* **2006**, *70*, 761−765.
(86) Carreira, L. A.; Maroni, V. A.; Swaine, J. W.; Plumb, R. C. *J. Chem. Phys.* **1966**, *45*, 2216−2220.
(87) Sipos, P.; May, P. M.; Hefter, G. *Dalton Trans.* **2006**, 368−375.
(88) Akitt, J. W.; Gessner, W. *J. Chem. Soc., Dalton Trans.* **1984**, *2*, 147−148.
(89) Graham, T. R.; Dembowski, M.; Martinez-Baez, E.; Zhang, X.; Jaegers, N. R.; Hu, J.; Gruszkiewicz, M. S.; Wang, H. W.; Stack, A. G.; Bowden, M. E.; Delegard, C. H.; Schenter, G. K.; Clark, A. E.; Clark, S. B.; Felmy, A. R.; Rosso, K. M.; Pearce, C. I. *Inorg. Chem.* **2018**, *57*, 11864−11873.
(90) Graham, T. R.; Semrouni, D.; Mamontov, E.; Ramirez-Cuesta, A. J.; Page, K.; Clark, A.; Schenter, G. K.; Pearce, C. I.; Stack, A. G.; Wang, H.-W. *J. Phys. Chem. B* **2018**, *122*, 12097−12106.
(91) Graham, T. R.; Han, K. S.; Dembowski, M.; Krzysko, A. J.; Zhang, X.; Hu, J.; Clark, S. B.; Clark, A. E.; Schenter, G. K.; Pearce, C. I.; Rosso, K. M. *J. Phys. Chem. B* **2018**, *122*, 10907−10912.
(92) Diakonov, I.; Pokrovski, G.; Schott, J.; Castet, S.; Gout, R. *Geochim. Cosmochim. Acta* **1996**, *60*, 197−211.
(93) Sipos, P.; Capewell, S. G.; May, P. M.; Hefter, G.; Laurenczy, G.; Lukács, F.; Roulet, R. *J. Chem. Soc., Dalton Trans.* **1998**, 3007−3012.
(94) Clark, S. B.; Buchanan, M.; Wilmarth, B. *Workshop on Environmental Management Report*; U.S. Department of Energy, Office of Science: Washington, DC, July 8−11, 2015.
(95) Sams, T. L.; Luke, J. J.; McClure, L. W. *Waste Management*; Symposium: Tucson, AZ, 2003.
(96) Barea, E.; Navarro, J. A.; Salas, J. M.; Masciocchi, N.; Galli, S.; Sironi, A. *J. Am. Chem. Soc.* **2004**, *126*, 3014−3015.
(97) Wang, L.; Zhou, H.; Hu, J.; Huang, B.; Sun, M.; Dong, B.; Zheng, G.; Huang, Y.; Chen, Y.; Li, L.; Xu, Z. *Science* **2019**, *363*, 265−270.
(98) Yang, C.; Nikiforidis, G.; Park, J. Y.; Choi, J.; Luo, Y.; Zhang, L.; Wang, S.-C.; Chan, Y.-T.; Lim, J.; Hou, Z.; Baik, M.-H.; Lee, Y.; Byon, H. R. *Adv. Energy Mater.* **2018**, *8*, No. 1702897.
(99) Park, M.; Ryu, J.; Wang, W.; Cho, J. *Nat. Rev. Mater.* **2016**, *2*, 16080.

https://dx.doi.org/10.1021/acs.analchem.0c04070
Anal. Chem. 2021, 93, 1068−1075